Sorptive Removal of [133]Ba from Aqueous Solution Using a Novel Cellulose Hydroxyapatite Composite Derived from Cigarette Waste

Vipul Vilas Kusumkar · Süleyman İnan [ORCID] **·
Michal Galamboš · Eva Viglašová · Martin Daňo**

Abstract [133]Ba is a hazardous radionuclide generated during the operation of nuclear power plants. [133]Ba needs to be removed from waste solutions because its half-life (10.55 years) and gamma energy pose a significant threat to human health. Cigarette butt (CB) is a waste that causes serious environmental problems. Various types of adsorbent materials are prepared based on the cellulose in its structure. The focus of the present study is to synthesize a novel composite material derived from CBs and to investigate its [133]Ba removal capability. Microfibrillated cellulose (MFC) obtained from CBs was modified with hydroxyapatite (HAp) via the co-precipitation method and converted into a composite adsorbent for the removal of [133]Ba ions. Response surface methodology (RSM) based on Box-Behnken Design (BBD) was employed for the examination of process variables such as initial pH, metal concentration, and adsorbent amount on [133]Ba sorption. XRD and FTIR data confirmed the successful isolation of cellulose and the modification of the cellulose surface with HAp. The model F-value (100.04) and R^2 (0.99) suggested that the proposed model was significant. Optimum conditions were determined as initial pH of 8, contact time of 134 min, and concentration of 0.01 mol/L, and the barium sorption capacity of MFC-HAp was found to be 0.75 mmol/g under these conditions. The maximum monolayer barium sorption capacity was determined to be 2.92 mmol/g. Combining cellulose and HAp to be a novel composite adsorbent is useful for reusing CB waste and promising for removing [133]Ba ions from aqueous solutions.

Keywords [133]Ba · Cigarette waste · Cellulose · Hydroxyapatite · Box-Behnken design · Sorption

V. V. Kusumkar · M. Galamboš · E. Viglašová
Faculty of Natural Sciences, Department of Nuclear Chemistry, Comenius University in Bratislava, Ilkovičova 6, 842 15 Bratislava, Slovakia

S. İnan (✉)
Ege University Institute of Nuclear Sciences, 35100 Bornova-İzmir, Türkiye
e-mail: suleyman.inan@ege.edu.tr

M. Daňo
Faculty of Nuclear Sciences and Physical Engineering, Department of Nuclear Chemistry, Czech Technical University in Prague, Břehová 7, 115 19 Prague, Czech Republic

1 Introduction

Nuclear waste is generated and released into the environment during activities such as nuclear reactor operation, mining, nuclear weapon production, and using radionuclides in medicine and research (Hu et al., 2010; Salbu et al., 2015). [133]Ba is a hazardous radionuclide produced during nuclear power generation and spent fuel reprocessing. It poses a significant threat to human health due to its half-life (10.55 y), gamma energy, and carcinogenic effects. In addition,

barium compounds are easily soluble in water and therefore can be transported over long distances. Therefore, the removal of ^{133}Ba from waste solutions and the safe management of barium-containing waste is of great importance (İnan et al., 2022).

Various approaches have been employed to eliminate radioactive pollutants from wastewater, including precipitation (Osmanlioglu, 2018), evaporation (Zaki et al., 2016), solvent extraction (McDowell et al., 1986; Xu et al., 2012), membrane separation (Combernoux et al., 2017; Kim et al., 2020), ion exchange (Möller et al., 2011; Roy et al., 2002), and adsorption (Celebi et al., 2009; Li et al., 2018; Zhao et al., 2022). In this regard, adsorption is garnering significant attention due to its high efficacy and ease of operation.

Global, daily consumption of cigarettes by smokers accounted for 967 million per day and almost 6.25 trillion cigarettes were burned throughout 2012 (Ng et al., 2014). The waste generated from cigarettes reached approximately 340-680 million kg/year, other than that 2.000.000 tons of paper, ink, cellophane, foil, and paste that are utilized for packaging purposes. Over 40% of all things gathered during metropolitan clean-ups and eliminated from public zones, for example, seashores, and stops are CBs and related products (Ariza et al., 2008; Bonanomi et al., 2015). The recycling of CBs is accomplished by physical, chemical, and physico-chemical processes. The recycled CBs give rise to secondary materials which can find application in many areas such as carbon dots (Anmei et al., 2018), bituminous mixtures (Toraldo et al., 2015), pesticides (Murugan et al., 2018) precast concrete bricks for paving (Wadalkar et al., 2018), hydrophobic adsorbent for oil-spill (Xiong et al., 2018), supercapacitors (Xiong et al., 2019), hydrogen storage materials (Blankenship & Mokaya, 2017), activated carbon for dye adsorption (Hamzah & Umar, 2017), asphalt concrete (Mohajerani et al., 2016), fired clay bricks (Sarani and Binti Abdul Kadir, 2013), and corrosion inhibitor extracts (Zhao et al., 2010).

A cigarette filter is a component of a cigarette and is typically made from cellulose acetate (CA). While CA is a biodegradable polymer, its degradation process is slow. According to Joly and Coulis (2018), it takes approximately 7.5 to 14 years for CA to completely decompose when present in compost and soil environments. CA can be converted into different forms of cellulose such as nanocellulose, cellulose nanocrystals (CNC), and microfibrillated cellulose (MFC). Cellulose has diverse applications in fields of research and technology, including but not limited to supercapacitors (Pérez-Madrigal et al., 2016) medical devices (Petersen & Gatenholm, 2011), drug delivery (Sun et al., 2019), wound healing (Kanikireddy et al., 2020), and adsorbents (Yue et al., 2019). For these reasons, cigarette waste is a viable source of cellulose material and the extraction of cellulose from cigarette waste has been carried out in many studies (De Fenzo et al., 2020; Ogundare et al., 2017).

The functional groups in the structure of cellulose have enabled them to be used in adsorption applications for various metal ions. However, numerous techniques for modifying and functionalizing cellulose have been proposed to enhance its adsorption capabilities. Some of these methods involve magnetic modification through a dipping process, acid, or alkali treatment, and incorporating other adsorbents onto the cellulose material.

Many studies have been reported in which modified cellulose was used for heavy metal removal. Saravanan and Ravikumar (2016) prepared Schiff base and carboxylic acid pendant cellulose for the removal of Cu(II) and Pb(II) ions. In another study, the bleached softwood Kraft pulp fibers were modified in carboxymethylated cellulose for the adsorption of Cu(II) and Ni(II) from an aqueous solution (Wang et al., 2019). Kim et al. (2017) prepared potassium copper hexacyanoferrate immobilized cellulose-based hydrogel for the adsorption of cesium ions from aqueous solution. To recover uranium ions from seawater, cellulose in sisal fiber has been modified by hydrothermal reaction in dilute phosphonate solutions (Tellería-Narvaez et al., 2020).

The approach of modifying material surfaces by incorporating other minerals or adsorbents has gained attention due to its several advantages, including easy synthesis, multifunctionality, and substantial enhancements. The use of cellulose as a sorbent for the removal of ^{133}Ba from radioactive waste comes with an intrinsic challenge because it is susceptible to radiolysis-induced decomposition, which results in the formation of isosaccharide species. The performance and stability of cellulose-based materials in radiochemistry uses are significantly influenced by this phenomenon, which has been well-documented in the literature (Diesen et al., 2017).

Hydroxyapatite (HAp) is a mineral that belongs to the apatite family, and it has gained significant attention from the scientific community as an optimal adsorbent material for capturing and recovering pollutants from water (Feng et al., 2010). High chemical stability is another benefit of using hydroxyapatite as a substance to immobilize nuclear waste. Even in harsh settings like nuclear waste repositories, this mineral is resistant to chemical deterioration (Zhou et al., 2021). Due to its exceptional surface characteristics, HAp has been widely and effectively employed for eliminating diverse types of contaminants from wastewater. Considering the properties of MFC and HAp, combining the two in a novel structure with superior properties may be a promising approach.

In this study, cellulose obtained from CBs was modified via HAp co-precipitation and a novel composite adsorbent was prepared. Characterization studies of materials were performed to enlighten the structural and textural differences. In addition, the effect of process variables, initial pH, metal concentration, and contact time on the removal of ^{133}Ba was analyzed by BBD. With this research, a new perspective is presented for the reusing of cigarette butt waste and the preparation of new composite materials for the removal of hazardous metal ions.

2 Materials and Methods

2.1 Materials

CBs were collected from public places near the Faculty of Science at Comenius University in Bratislava, Slovakia. Sodium hydroxide pellets (NaOH, ≥99%, M: 40.00 g/mol), sulfuric acid (H_2SO_4, 98%, M: 98.08 g/mol), ethanol (C_2H_5OH, 96%, M: 46.07 g/mol), sodium chlorite ($NaClO_2$, 25%, M: 90.44 g/mol), di-ammonium hydrogen phosphate [$(NH_4)_2HPO_4$, 99%, M: 132.06 g/mol], calcium nitrate tetrahydrate [$Ca(NO_3)_2 \cdot 4H_2O$, 99%, M: 236.15 g/mol], barium chloride ($BaCl_2$, 99.90%, M: 208.23 g/mol), ammonia solution (NH_4OH, 25%, M: 35.05 g/mol), acetic acid (CH_3COOH, 100%, M: 60.05 g/mol), and phosphoric acid (H_3PO_4, 85%, M: 98.00 g/mol) were purchased from Sigma-Aldrich (USA). All chemicals were of analytical grade and were used without any further purification.

Radiotracer concentration was as follows: ^{133}Ba in the form of [^{133}Ba] $BaCl_2$ (Eurostandard CZ s.r.o., Czech Republic) with a volume activity of 2 MBq/mL.

2.2 Instrumentation

X-Ray Powder Diffraction (XRD) analysis was performed by Miniflex600 (Rigaku, Tokyo, Japan). The applied voltage was equal to 40 kV with a current of 15 mA. The lower limit of the angle range was set to $2\theta = 3°$ because of the organic content in samples. The upper limit is $2\theta = 80°$. The angular velocity of the detector was chosen to be $3° \cdot min^{-1}$. The FTIR-ATR instrument was used to acquire spectra in the range of 400–4000 cm^{-1} using Fourier Transform Infrared Spectroscopy (FTIR).

2.3 Preparation of Microfibrillated Cellulose (MFC)

2.3.1 Conditioning of CBs

The collected CBs were thoroughly washed several times with water to remove ash and tobacco. The washed CBs were soaked in water to remove the paper from the filter of the CB. In the next step, the burnt tips of the CBs were chopped using a scissor and washed with water. These cleaned CBs were kept in an oven at 30 °C for drying. Dried CBs (10 g) were washed with ethanol using a magnetic stirrer at 800 rpm for 8 h. Following this, ethanol removal was achieved by washing the filters several times with deionized water. Then, filters were kept in the oven at 30 °C for 4 h. In the next step, the conditioned filters were sorted and used.

2.3.2 Cleaving of Acetyl Group and Bleaching of CBs

Cigarette filters are made from cellulose acetate. The cleavage of the acetyl group is important to obtain cellulose. In this procedure, obtained cigarette strands were treated with 5% NaOH at 60 °C for 6 h. Then, they were neutralized with deionized water and dried at 30 °C in an oven. In the bleaching step, CBs were bleached using 15 g NaOH, 40 mL of acetic, and 1.7% $NaClO_2$ in 500 ml water for 6 h at 800 rpm on a magnetic stirrer.

2.3.3 Acid hydrolysis

In this step, acid hydrolysis of CBs was performed using sulfuric acid. The CBs were treated with 10 mol/L 100 mL sulfuric acid for 60 min at 40 °C on a magnetic stirrer. The diagram in Fig. 1a illustrates the preparation steps of MFC starting from CB waste.

2.4　Preparation of MFC-HAp Composite

The first step involved a phosphorylation reaction, as depicted in Fig. 1b. Initially, 3 g of the filtered sample was treated with 75% weight of phosphoric acid at 70 °C for 5 h. To terminate the reaction, distilled water was added, and the unreacted chemicals were eliminated by washing with a mixture of water and ethanol. The resulting MFC was then dried in an oven for 24 h at 30 °C (Bonanomi et al., 2015).

In the following step, 10% of phosphorylated MFC (P-MFC) was mixed with water, and 5.7 g of $Ca(NO_3)_2 \cdot 4H_2O$ was added. Then, the solution pH was adjusted to around 10, and 1.6 g $(NH_4)_2HPO_4$ was added dropwise into the solution. The temperature of the mixture was increased to 80 °C and stirred for 5 h at 800 rpm in a magnetic stirrer. The prepared precipitate was washed several times until the pH of the filtrate was neutral. Finally, the composite was dried and used for further studies (Ariza et al., 2008).
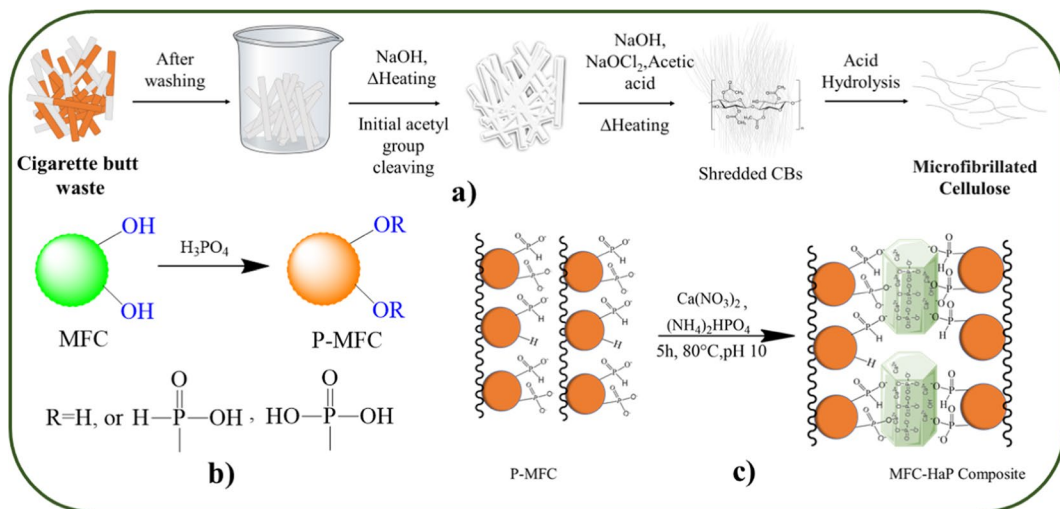
A schematic representation of MFC-HAp synthesis is given in Fig. 1c.

2.5　Batch Sorption Experiments

Sorption studies of ^{133}Ba on MFC-HAp composite were performed by radioisotope indication method using radioisotope of ^{133}Ba. The sorption experiments were conducted using the batch method, with aerobic conditions maintained at laboratory temperature. The influence of various parameters on sorption was evaluated by introducing 5 mL of the aqueous phase into a plastic tube containing 0.05 g of MFC-HAp. MFC-HAp and the aqueous phase were mixed in a laboratory extractor with a constant speed of mixing. Following ^{133}Ba sorption, centrifugation was applied at a speed of 8000 rot/min for 15 min. Subsequently, a portion of each resulting supernatant was collected and subjected to analysis using a Modumatic model gamma spectrometer equipped with a NaI(Tl) detector. The area of the 356 keV photopeak for ^{133}Ba was analyzed. The measurement's statistical error was less than 5%. The following equations were used to calculate the ^{133}Ba sorption properties of MFC-HAp:

Equilibrium concentration (C_{eq})

$$C_{eq} = \frac{C_0 \times a}{a_0}(mol/L) \tag{1}$$

Fig. 1 **a** The preparation steps of MFC from cigarette butt waste, **b** Phosphorylation of MFC, **c** Schematic representation of MFC-HAp synthesis

Distribution coefficient (K_d)

$$K_d = \frac{(a_0 - a)}{a} \times \frac{V}{m}(\text{mL/g}) \qquad (2)$$

Sorption capacity (q)

$$q = K_d \times C_{eq}(\text{mmol/g}) \qquad (3)$$

In the above Eqs, C_0 is the initial concentration of the solute in aqueous phase (mol/L), C_{eq} is the equilibrium concentration of the solute in aqueous phase (mol/L), V is the volume of the aqueous phase (mL), m is the mass of sorbent (g), a_0 is the initial volume activity of solution (Bq/mL), a is the equilibrium volume activity of solution (Bq/mL), and K_d is the distribution coefficient (mL/g).

2.6 Experimental Design

The operational parameters on the sorptive removal of [133]Ba were optimized using BBD based on RSM. The influence of process variables namely initial pH (A), contact time (B), and metal concentration (C) on [133]Ba sorption was examined by conducting 17 experimental runs at 3 levels (low, center, high). Table 1 summarizes the variables, levels, and ranges employed in the design. Equation (4) shows the model equation which includes both linear and quadratic terms for estimating the optimal response.

$$\begin{aligned} y = &b_0 + b_1A + b_2B + b_3C + b_{11}A^2 + b_{22}B^2 \\ &+ b_{33}C^2 + b_{12}AB + b_{13}AC + b_{23}BC \end{aligned} \qquad (4)$$

In Eq. (4), y represents the response ([133]Ba sorption capacity), $A, B,$ and C are the coded variables. The coefficients associated with intercept term, linear, quadratic, and dual interaction effects are denoted as $b_0, b_1, b_2, b_3, b_{11}, b_{22}, b_{33},$ and $b_{12}, b_{13},$

b_{23}, respectively. The data was subjected to statistical, regression, and graphical analysis using Design-Expert 13 software, developed by State Ease Inc. (USA).

## 3 Results and Discussion

3.1 Characterization Studies

The XRD pattern of MFC (Fig. 2a) showed intense peaks at around $2\theta = 12°$ (101), 20° (101), and 22° (002). The data was attributed to cellulose II-type structure and identified by the Joint Committee on Powder Diffraction Standards (JCPDS) standard PDF card 00–056-1717. The XRD pattern of the MFC-HAp composite in Fig. 2b illustrates that the obtained crystalline phase is assigned to hydroxyapatite. Hydroxyapatite peaks at crystal planes (002), (211), (112), (301), (310), (222), and (213) correspond to the JCPDS standard PDF card No. 01–071-5049 for hydroxyapatite (Fu et al., 2016; Miskovic-Stankovic et al., 2015).

FT-IR method was used for the identification of change in surface functional groups of the CBs and derived products. In Fig. 3, we compared the transmittance of CBs, MFC, P-MFC, MFC-HAp, and commercial hydroxyapatite. In CB, MFC, P-MFC, and MFC-HAp, typical cellulose bonds are observed at 3350 cm^{-1} for the -OH groups, 2903 cm^{-1} for the -CH$_2$, 1639 cm^{-1} for the H-O-H due to moisture present in the sample, 1380 cm^{-1} for the -CH, 1160 cm^{-1} for -C-O-C stretching, 1054 cm^{-1} for the -C-O-C- bending vibrations of glycosidic units or from β-(1 → 4)-glycosidic bonds (Fan et al., 2012). MFC formation can be confirmed by reduced area of transmittance around 3300 to 3380 cm^{-1} of hydroxy groups due to acid hydrolysis. To confirm the phosphorylation of MFCs, a band at 1268 cm^{-1} indicates P = O stretching mode, while the bands at 986 cm^{-1} and 876 cm^{-1} are attributed to the presence of P-OH in P-MFC (Anmei et al., 2018). Poralan et al. (2015) reported that the strong peaks typically seen in the 900–1200 cm^{-1} range were associated with the stretching vibrations of the PO$_4$ tetrahedra. In Fig. 3, it can be observed that the sharp peak for the phosphate group was obtained at around 1030 cm^{-1}

Table 1 Variables, levels, and ranges used in BBD

Variable	Unit	Code	Level		
			−1 (low)	0 (center)	+1 (high)
Initial pH	-	A	3	5.5	8
Contact time	min	B	5	92.5	180
Concentration	mol/L	C	0.00001	0.005005	0.01

Fig. 2 XRD curves of synthesized materials. (**a**) MFC, (**b**) MFC-HAp composite
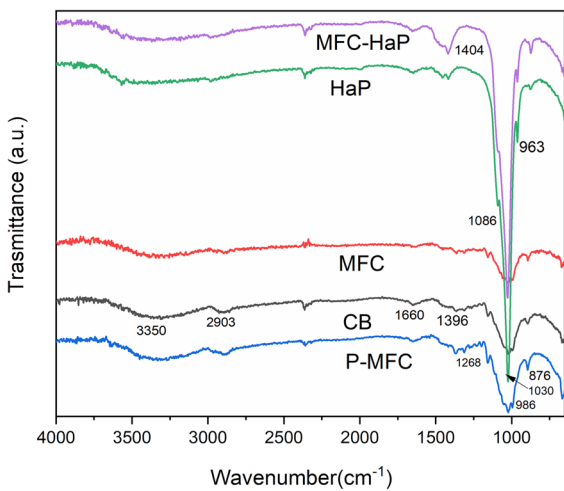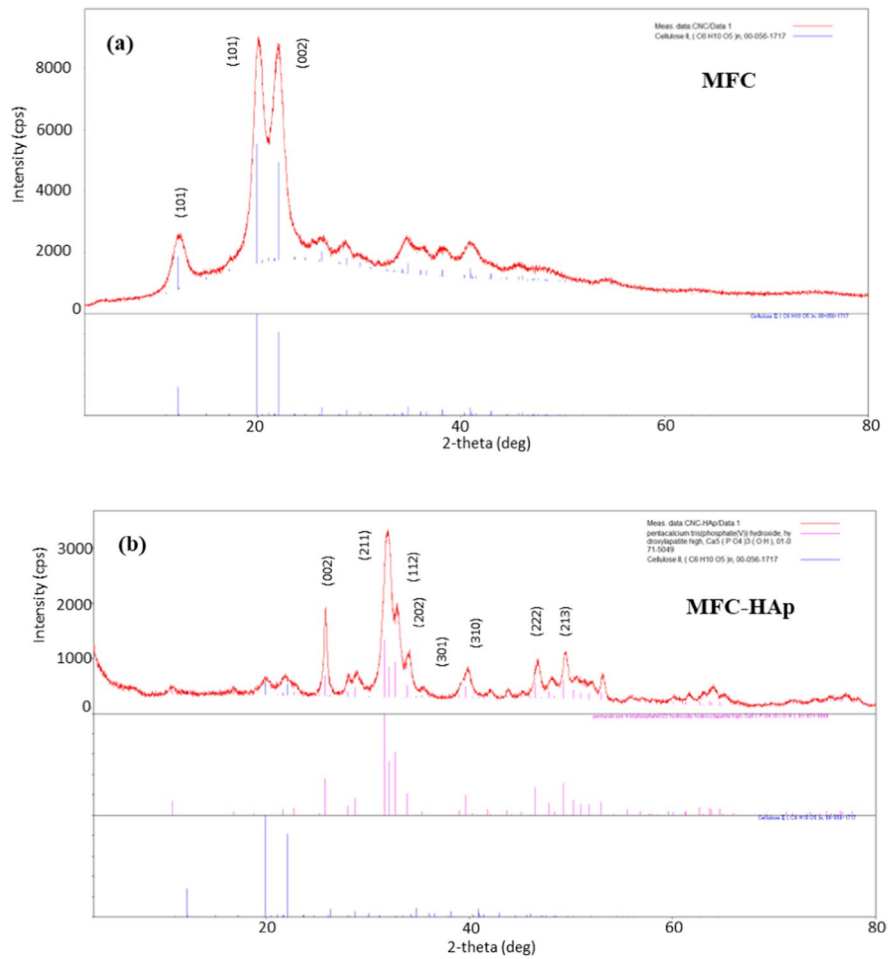
Fig. 3 FT-IR spectra of CB, MFC, P-MFC, HAp, and MFC-HAp

for MFC-HAp and commercial HAp. However, in MFC-HAp, the intensity of the PO_4^{3-} peak is lower than that of HAp.

3.2 Optimization by BBD

BBD matrix consists of 12 factorial and 5 replicate runs. Table 2 presents the experimental variables as well as the predicted and experimental responses. The relationship between the independent variables and response was modeled using a second-order polynomial equation. To predict the sorption capacity of ^{133}Ba, the empirical model specified in Eq. (5) was utilized.

$$y = 0.39 + 0.01A + 0.02B + 0.34C + 0.01AB$$
$$+ 0.02AC + 0.03BC - 0.01A^2 - 0.06B^2 - 0.01C^2$$
$$(5)$$

Table 2 BBD matrix, experimental and predicted responses

Run	A: Initial pH	B: Contact time (min)	C: Concentration (mol/L)	Experimental Response Sorption Capacity (mmol/g)	Predicted Response Sorption Capacity (mmol/g)
1	5.5	92.5	0.005005	0.3787	0.3887
2	3	5	0.005005	0.3283	0.3134
3	5.5	180	0.01	0.6875	0.7027
4	5.5	5	0.01	0.5893	0.6229
5	3	92.5	0.00001	0.0008	0.0310
6	5.5	92.5	0.005005	0.3943	0.3887
7	5.5	180	0.00001	0.0010	− 0.0327
8	5.5	92.5	0.005005	0.4089	0.3887
9	8	92.5	0.00001	0.0008	0.0196
10	3	180	0.005005	0.3148	0.3183
11	3	92.5	0.01	0.7031	0.6844
12	5.5	5	0.00001	0.0009	− 0.0143
13	5.5	92.5	0.005005	0.4045	0.3887
14	5.5	92.5	0.005005	0.3573	0.3887
15	8	92.5	0.01	0.7689	0.7388
16	8	180	0.005005	0.3506	0.3655
17	8	5	0.005005	0.3126	0.3091

ANOVA is a statistical method commonly used to assess the significance of a regression model, including the quadratic model. Table 3 contains the ANOVA results for the regression parameters of the quadratic model. In general, larger F-values and smaller P-values indicate that the corresponding parameter is more significant. The present regression model was determined statistically significant with a F-value of 100.04 and a P-value of < 0.0001. The P-value indicates that there is only a 0.01% chance that the F-value was the result of random variation or noise.

The lack-of-fit analysis is used to assess the validity of a model. In this case, the fact that the P-value

Table 3 ANOVA for quadratic model

Source	Sum of Squares	df	Mean Square	F-value	p-value	R^2
Model	0.9636	9	0.1071	100.04	< 0.0001	0.99
A-Initial pH	0.0009	1	0.0009			
B-Contact time	0.0019	1	0.0019			
C-Concentration	0.9420	1	0.9420			
AB	0.0007	1	0.0007			
AC	0.0011	1	0.0011			
BC	0.0024	1	0.0024			
A^2	0.0002	1	0.0002			
B^2	0.0130	1	0.0130			
C^2	0.0008	1	0.0008			
Residual	0.0075	7	0.0011			
Lack of Fit	0.0057	3	0.0019	4.30	0.0964	
Pure Error	0.0018	4	0.0004			
Cor Total	0.9711	16				

for the lack-of-fit is 0.0964, which is greater than the commonly used threshold of 0.05, suggests that the quadratic model has successfully established a precise functional relationship between the response and the independent variables. Furthermore, the high value of R^2 (0.99) indicates that there is a strong correlation between the actual and predicted values, which indicates that the fitting of the model is good. The R^2 value obtained suggests that the regression model effectively predicted and explained the relationship between the independent variables and the response. Specifically, the model was able to account for 99% of the total variation observed in the sorption of ^{133}Ba, leaving only 1% of residual variability.

The adjusted R^2 and predicted R^2 are two measures used to evaluate a model's performance. The adjusted R^2, with a value of 0.98, assesses the proportion of variation in the data that can be attributed to the model. On the other hand, the predicted R^2, with a value of 0.90, evaluates the model's ability to accurately predict experimental response values. To achieve reasonable agreement, the difference between the adjusted R^2 and predicted R^2 should be less than 0.20. A larger difference could indicate potential errors in either the experimental data or the predicted model. In this study, the small difference of 0.08 between the adjusted R^2 and predicted R^2 suggests

that the model is performing well and there is a strong agreement between the two metrics.

Figure 4 shows a plot comparing the actual experimental response, which is the sorption capacity, with the predicted response generated by the RSM-BBD model. The plot demonstrates that the data points closely follow the linear line, indicating that the model was able to adequately explain the range of the experimental conditions studied.

The coefficients and P-values of the main, dual, and quadratic effects of independent variables are listed in Table 4. A term in a statistical analysis is considered to be statistically significant if its associated P-value is less than 0.05. In Table 4, C and B^2 were the statistically significant model terms, while A, B, AB, AC, BC, A^2, and C^2 have no statistically significant effect on sorption. In regression analysis, the positive sign of the coefficient in the model equations indicates that the relevant term affects adsorption positively, and the negative sign of the coefficient indicates that adsorption is negatively affected by the term. Since the coefficient values for initial pH ($A = 0.01$), contact time ($B = 0.02$), and concentration ($C = 0.34$) are positive, they can be interpreted as having an increasing effect on sorption capacity. Similar interpretations are made in studies based on experimental design (Adetokun et al., 2019; Hasan et al., 2009; Muntean et al., 2023). The change in sorption

Fig. 4 Predicted versus actual responses

Table 4 Coefficients and P-values of parameters

	Coefficient	df	Standard Error	P-value
Intercept	0.39	1	0.0146	
A-Initial pH	0.01	1	0.0116	0.3843
B-Contact time	0.02	1	0.0116	0.2263
C-Concentration	0.34	1	0.0116	<0.0001
AB	0.01	1	0.0164	0.4571
AC	0.02	1	0.0164	0.3482
BC	0.03	1	0.0164	0.1773
A^2	−0.01	1	0.0159	0.6872
B^2	−0.06	1	0.0159	0.0103
C^2	−0.01	1	0.0159	0.4212

capacity depending on the main effects is given in Fig. 5a-c.

A slight increase in the sorption capacity could be observed with the increase in pH. Capacity values were found to be 0.371 and 0.392 mmol/g at pH 3 and pH 8, respectively, and reached a maximum of 0.393 mmol/g at pH 7.5 (Fig. 5a). In Fig. 5b, the effect of contact time can be examined in two parts. Over the 5-105 min range, the ^{133}Ba uptake capacity increased from 0.318 to 0.389 mmol/g. A slight decrease in uptake capacity was observed after 105 min and it was obtained as 0.349 mmol/g at 180 min. Unlike other variables, concentration has a strong influence on the sorption capacity (Fig. 5c). With the increase in barium concentration, the barium uptake capacity increased significantly. By increasing the concentration from 0.00001 to 0.01 mol/L, the capacity increased from 0.032 to 0.72 mmol/g.

The binary interactions of process variables are represented by 3D surface plots. The variation of sorption capacity depending on pH-contact time, pH-concentration, and contact time-concentration binary interactions is shown in Fig. 6a-c. In each surface graph, two variables are changed while the value of the other variable is kept at the center level. Figure 6a shows the variation of sorption capacity depending on initial pH (A) and contact time (B). Maximum q was found to be 0.396 mmol/g at initial pH 8 and contact time of 115 min by fixing the concentration at 0.005005 mol/L. Figure 6b demonstrates the interaction between initial pH (A) and metal concentration (C). Maximum q was obtained as 0.739 mmol/g at initial pH 8 and concentration of 0.01 mol/L by holding

the contact time at 92.5 min. Figure 6c presents the dependency of sorption on contact time (B) and metal concentration (C). Maximum q of 0.725 mmol/g was obtained at contact time 124 min and concentration of 0.01 mol/L by fixing initial pH at 5.5.

3.3 Sorption Mechanisms of Ba^{2+} Ions on MFC-HAp Composite

The sorption of the Ba^{2+} ion on the MFC-HAp composite can be explained in two different pathways via ion exchange and surface complexation. The ion exchange phenomenon in hydroxyapatite generally hinges on the size of the metal cation. According to prevailing theories, successful ion exchange is likely when the size of the cation does not deviate by more than 15% from that of the Ca^{2+} ion, which has a radius of 0.099 nm (Saleeb & De Bruyn, 1972). The size of the Ba^{2+} ion, at 0.149 nm, significantly differs from the requisite size for effective exchange. However, Reichert and Binner (1996) have contended that ions with a radius exceeding this limit can still participate in the exchange process within the hydroxyapatite lattice, challenging the earlier stipulation. Importantly, it is noteworthy that ion exchange does not solely occur on the surface of hydroxyapatite; it also takes place within the natural channels, specifically Ca (II) and Ca (I), within the hydroxyapatite lattice (Monteil-Rivera & Fedoroff, 2015). The following equation depicts the possible ion exchange (Skwarek & Janusz, 2019).

$$Ca_{10}(PO_4)_6(OH)_2 + xBa^{2+} \leftrightarrow Ca_{10-x}Ba_x(PO_4)_6(OH)_2 + xCa^{2+}$$
(6)
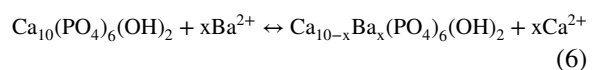
The synergistic interaction of hydroxyl groups and phosphate groups on the composite's surface enables the surface complex phenomenon for Ba^{2+} ion removal in MFC-HAp composites, providing multiple binding sites for Ba^{2+} ions. Hydroxyl groups from cellulose microfibers and hydroxyapatite participate in surface reactions with Ba^{2+} ions, while phosphate groups from hydroxyapatite improve complexation by providing additional anchoring points (Ferri et al., 2019). The complementary binding properties of these functional groups cause this synergistic effect. The hydroxyl groups and phosphate groups provide multidentate coordination sites, allowing for stronger binding interactions with Ba^{2+} ions.

Fig. 5 The relationship between main effects and ^{133}Ba sorption capacity. (**a**) effect of initial pH, (**b**) effect of contact time, (**c**) effect of concentration
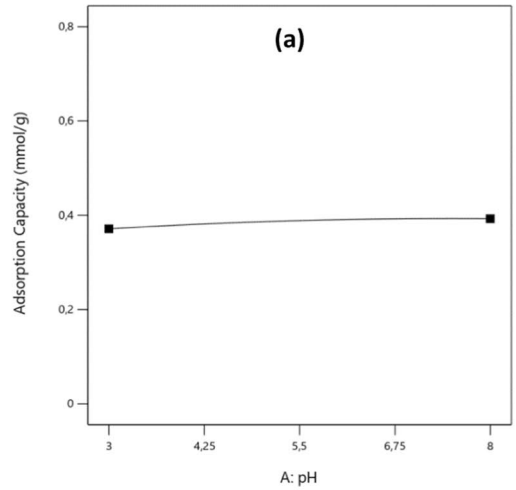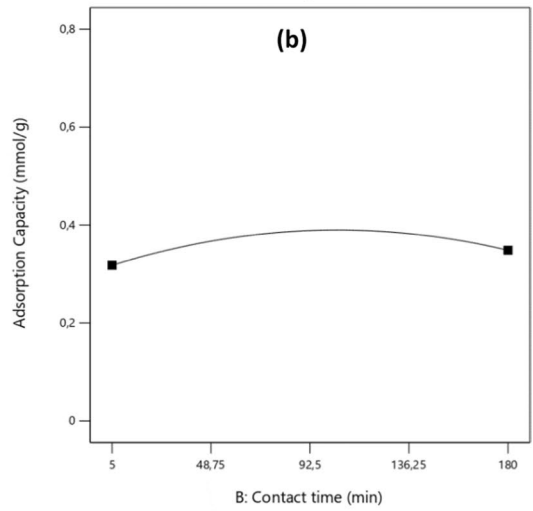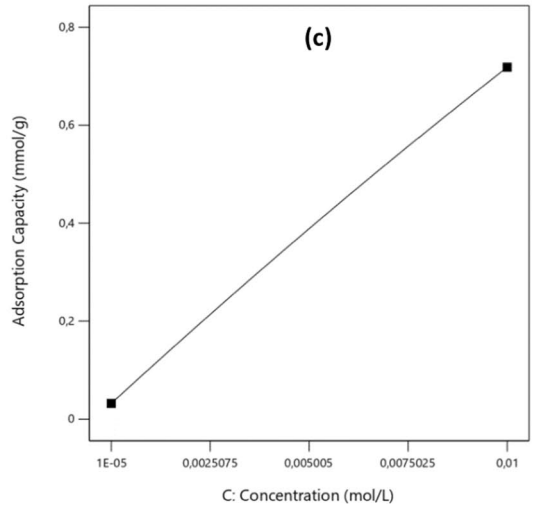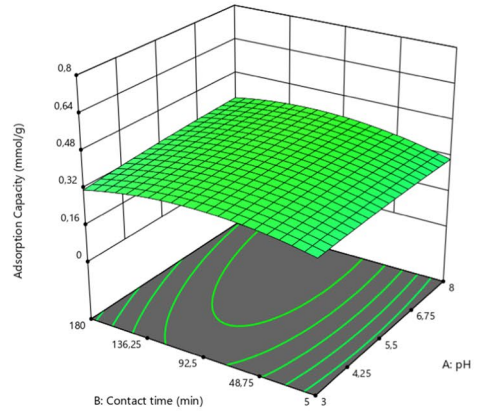
Fig. 6 3D response surface plots for binary interactions of process variables. (**a**) initial pH and contact time, (**b**) initial pH and concentration, (**c**) contact time and concentration
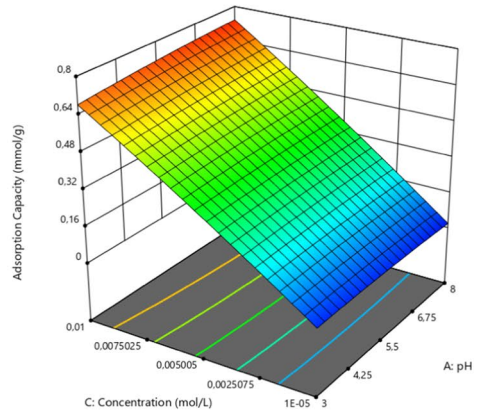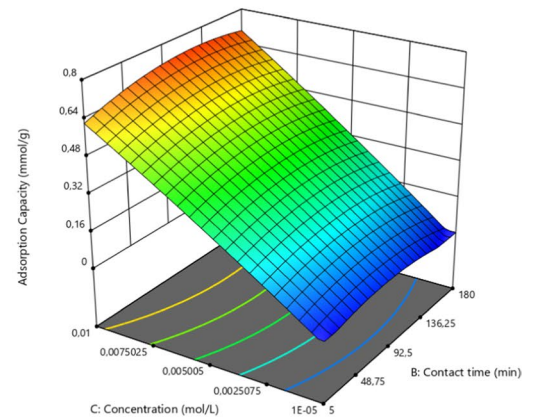
3.4 Effect of Metal Concentration and Isotherm Study

An adsorption isotherm describes the correlation between the degree of adsorption and the concentration of the adsorbed species while keeping the temperature constant. Giles et al. (1974) categorized adsorption isotherms into four primary groups: L (Langmuir-type), H (high affinity), S (cooperative), and C (constant partition). The sorption isotherm curve for Ba^{2+} in Fig. 7a exhibits a closer resemblance to the H-type, indicating a remarkably high affinity between the adsorbate and adsorbent. Consequently, in dilute solutions, the adsorbate is nearly entirely adsorbed.

The relationship between the concentration of Ba^{2+} ions and the uptake capacity of the sorbent was investigated over a concentration range of 1×10^{-5} to 5×10^{-2} mol/L. The results showed that as the concentration of Ba^{2+} ions in the solution increased, the sorbent's uptake capacity also increased. When the concentration was 5×10^{-2} mol/L, the rate of increase in capacity slowed down, and uptake capacity was calculated as 2.59 mmol/g.

The Langmuir model assumes that the adsorption of a species onto a surface occurs at specific homogeneous sites and is limited to the formation of a single adsorbate layer. The linearized form of the Langmuir equation can be written as follows (Langmuir, 1918):

$$\frac{C_e}{q_e} = \frac{C_e}{q_m} + \frac{1}{q_m \times b} \tag{7}$$
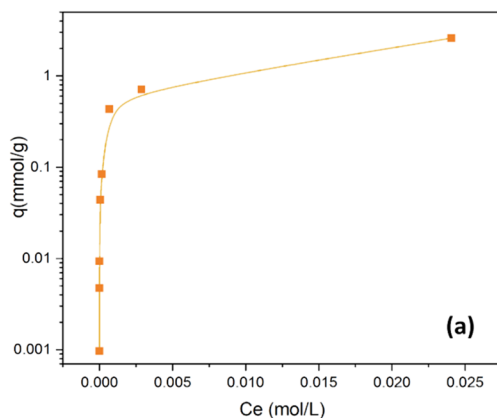
In Eq. (7), q_e is the amount of metal ions adsorbed at equilibrium (mol/g), C_e is the concentration of metal ions in the solution at equilibrium (mol/L), q_m is the monolayer adsorption capacity (mol/g), and b is the constant related to the free energy of adsorption. Langmuir parameters and R^2 value are presented in Table 5. The Langmuir model was used to fit the experimental data, and a reasonably good fit was observed based on the R^2 value. This indicates that the sorption on the surface might occur as a monolayer coverage. The maximum monolayer barium sorption capacity was determined to be 2.92 mmol/g.

Multilayer sorption on heterogeneous surfaces can be described by the Freundlich model (Freundlich, 1907). It is written in its linear form as,

$$logq_e = logK_f + \frac{1}{n} \times logC_e \tag{8}$$

In Eq. (8), a constant K_f (mol/g) is associated with the adsorption capacity, and a parameter $1/n$ is dependent on the adsorption intensity. Based on the

Table 5 Langmuir and Freundlich isotherm model parameters

Model	Parameter	Value
Langmuir	q_m (mol/g)	2.92×10^{-3}
	b	263
	R^2	0.915
Freundlich	$1/n$	0.72
	K_f	48.24
	R^2	0.993
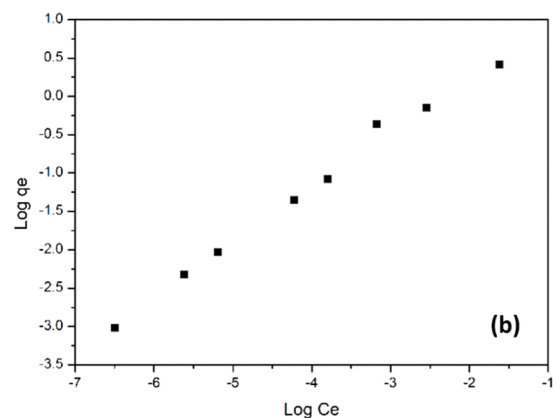
Fig. 7 (**a**) Influence of metal concentration on [133]Ba uptake capacity, (**b**) Freundlich isotherm (Initial pH: 6.4; contact time: 180 min; dosage: 10 g/L; temperature: ambient conditions)

Table 6 Comparison of some adsorbents used in Ba^{2+} sorption

Sorbent material	Initial pH	Concentration	q (mmol/g)	Reference
Copper ferrite/reduced graphene oxide (CG)	7	N/A	1.18	Mary et al., 2022
CS-HMF	6	10–300 mg/L	0.47	Liakos et al., 2021
Alk-$Ti_3C_2T_x$	7	50–500 mg/L	0.34	Mu et al., 2018
Synthetic Allophane-1	8.5	1–100 mg/L	0.28	Baldermann et al., 2018
Synthetic hydroxyapatite	7.5	1×10^{-6}-1×10^{-3} mol/L	0.038	Skwarek & Janusz, 2019
Ash based sorbent (Z 90–15)	4	10–1000 mg/L	0.87	Noli et al., 2016
Iranian expanded perlite	6	3.6×10^{-5}-3.6×10^{-4} mol/L	0.018	Torab-Mostaedi et al., 2011
Greek bentonite	4	50–1000 mg/L	0.41	Noli et al., 2021
Ferrihydrite	8	5×10^{-6}-5×10^{-4} mol/L	~0.1	Sajih et al., 2014
Goethite	10	5×10^{-6}-5×10^{-4} mol/L	~0.01	
Granitic rock-Biotite	8.6	1×10^{-9}-1×10^{-3} mol/L	2.86×10^{-5}	Muuri et al., 2018
MFC-HAp	8	1×10^{-5}-5×10^{-2} mol/L	2.92	Present work

information presented in Fig. 7b and Table 5, it can be concluded that the data for Ba^{2+} sorption conforms well to the Freundlich model. The calculated values for the constant K_f and the parameter $1/n$ were 48.24 and 0.72, respectively. The obtained value for $1/n$, which was between 0 and 1, suggests that the sorption of Ba^{2+} onto the MFC-HAp composite was favorable under the given working conditions.

Table 6 provides an overview of the Ba^{2+} sorption capacities of different sorbent types used for the treatment of aqueous solutions and radioactive wastes in acidic to alkaline media. The MFC-HAp composite has a high affinity for Ba^{2+} compared to other materials reported in the literature.

4 Conclusion

In this study, we report the synthesis of novel cigarette waste-derived microfibrillated cellulose (MFC)-hydroxyapatite (HAp) composite and its use for the removal of radiobarium from aqueous solution. The successful isolation of MFC from cigarette waste and the preparation of the MFC- HAp composite was confirmed by XRD and FTIR analyses. The experimental tests for [133]Ba sorption were designed and executed by RSM based on BBD. As a result of the experiments carried out using the BBD, the proposed regression model with a F-value of 100.04 explained the sorption successfully. Since the P-value was very low ($P < 0.05$), the effect of the concentration parameter on the sorption was found to be significant. The positive value of the coefficient related to the concentration ($b_C = 0.34$) indicates that the barium uptake capacity increases with the increase in the concentration. The uptake capacity of MFC-HAp was found to be 0.75 mmol/g under optimum conditions as initial pH of 8, contact time of 134 min, and concentration of 0.01 mol/L. The experimental sorption data showed better agreement with the Freundlich model and the monolayer sorption capacity from Langmuir isotherm was found to be 2.92 mmol/g.

In conclusion, an already abundant waste has been converted into a composite material that can be used to remove a hazardous pollutant. This new material has shown an effective performance in removing [133]Ba from aqueous solutions.

Data Availability   The manuscript has no associated data.

Declarations

Ethical Approval   Ethical approval is not applicable for this article.

Consent to Participate   As part of this study, no human or animal participants were involved at any stage.

Consent to Publish   All authors have approved the manuscript before submission and agree to publication.

Competing Interests   The authors declare no competing interests.

References

Adetokun, A. A., Uba, S., & Garba, Z. N. (2019). Optimization of adsorption of metal ions from a ternary aqueous solution with activated carbon from Acacia senegal (L.) Willd pods using Central Composite Design. *Journal of King Saud University - Science, 31*(4), 1452–1462. https://doi.org/10.1016/j.jksus.2018.12.007

Anmei, S., Qingmei, Z., Yuye, C., & Yilin, W. (2018). Preparation of carbon quantum dots from cigarette filters and its application for fluorescence detection of Sudan I. *Analytica Chimica Acta, 1023*, 115–120. https://doi.org/10.1016/j.aca.2018.03.024

Ariza, E., Jiménez, J. A., & Sardá, R. (2008). Seasonal evolution of beach waste and litter during the bathing season on the Catalan Coast. *Waste Management, 28*, 2604–2613. https://doi.org/10.1016/j.wasman.2007.11.012

Baldermann, A., Griessbacher, A. C., Baldermann, C., Purgstaller, B., Letofsky-Papst, I., Kaufhold, S., & Dietzel, M. (2018). Removal of barium, cobalt, strontium, and zinc from solution by natural and synthetic allophane adsorbents. *Geosciences, 8*(9), 309. https://doi.org/10.3390/geosciences8090309

Blankenship, T. S., & Mokaya, R. (2017). Cigarette butt-derived carbons have ultra-high surface area and unprecedented hydrogen storage capacity. *Energy and Environmental Sciences, 10*, 2552–2562. https://doi.org/10.1039/D1EE90031E

Bonanomi, G., Incerti, G., Cesarano, G., Gaglione, S. A., & Lanzotti, V. (2015). Cigarette butt decomposition and associated chemical changes assessed by ^{13}C CPMAS NMR. *PLoS ONE, 27*(10), e0117393. https://doi.org/10.1371/journal.pone.0117393

Celebi, O., Kilikli, A., & Erten, H. N. (2009). Sorption of radioactive cesium and barium ions onto solid humic acid. *Journal of Hazardous Materials, 168*, 695–703. https://doi.org/10.1016/j.jhazmat.2009.02.090

Combernoux, N., Schrive, L., Labed, V., Wyart, Y., Carretier, E., & Moulin, P. (2017). Treatment of radioactive liquid effluents by reverse osmosis membranes: From lab-scale to pilot-scale. *Water Research, 123*, 311–320. https://doi.org/10.1016/j.watres.2017.06.062

De Fenzo, A., Giordano, M., & Sansone, L. (2020). A clean process for obtaining high-quality cellulose acetate from cigarette butts. *Materials, 13*, 4710. https://doi.org/10.3390/ma13214710

Diesen, V., Forsberg, K., & Jonsson, M. (2017). Effects of cellulose degradation products on the mobility of Eu (III) in repositories for low and intermediate level radioactive waste. *Journal of Hazardous Materials, 340*, 384–389. https://doi.org/10.1016/j.jhazmat.2017.07.008

Fan, M., Dai, D., & Huang, B. (2012). Fourier transform infrared spectroscopy for natural fibres. In S. Salih (Ed.), *Fourier transform - materials analysis* (pp. 45–38). InTech. https://doi.org/10.5772/35482

Feng, Y., Gong, J. L., Zeng, G. M., Niu, Q. Y., Zhang, H. Y., Niu, C. G., Deng, J. H., & Yan, M. (2010). Adsorption of Cd(II) and Zn(II) from aqueous solutions using magnetic hydroxyapatite nanoparticles as adsorbents. *Chemical Engineering Journal, 162*(2), 487–494. https://doi.org/10.1016/j.cej.2010.05.049

Ferri, M., Campisi, S., Scavini, M., Evangelisti, C., Carniti, P., & Gervasini, A. (2019). In-depth study of the mechanism of heavy metal trapping on the surface of hydroxyapatite. *Applied Surface Science, 475*, 397–409. https://doi.org/10.1016/j.apsusc.2018.12.264

Freundlich, H. (1907). Über die adsorption in lösungen. *Zeitschrift Für Physikalische Chemie, 57*(1), 385–470. https://doi.org/10.1515/zpch-1907-5723

Fu, L.-H., Liu, Y.-J., Ma, M.-G., Zhang, X.-M., Xue, Z.-M., & Zhu, J.-F. (2016). Microwave-assisted hydrothermal synthesis of cellulose/hydroxyapatite nanocomposites. *Polymers, 8*, 316. https://doi.org/10.3390/polym8090316

Giles, C. H., Smith, D., & Huitson, A. (1974). A general treatment and classification of the solute adsorption isotherm part. I. Theoretical. *Journal of Colloid and Interface Science, 47*(3), 755–765. https://doi.org/10.1016/0021-9797(74)90252-5

Hamzah, Y., & Umar, L. (2017). Preparation of creating active carbon from cigarette filter waste using microwave-induced KOH activation. *Journal of Physics: Conference Series, 853*(1), 012027. https://doi.org/10.1088/1742-6596/853/1/012027

Hasan, S. H., Srivastava, P., & Talat, M. (2009). Biosorption of Pb(II) from water using biomass of Aeromonas hydrophila: Central composite design for optimization of process

variables. *Journal of Hazardous Materials, 168*(2–3), 1155–1162. https://doi.org/10.1016/j.jhazmat.2009.02.142

Hu, Q.-H., Weng, J.-Q., & Wang, J.-S. (2010). Sources of anthropogenic radionuclides in the environment: A review. *Journal of Environmental Radioactivity, 101*, 426–437. https://doi.org/10.1016/j.jenvrad.2008.08.004

İnan, S., Kusumkar, V. V., Galamboš, M., Viglašová, E., Rosskopfová, O., & Daňo, M. (2022). Isotherm, kinetic, and selectivity studies for the removal of ^{133}Ba and ^{137}Cs from aqueous solution using Turkish Perlite. *Materials, 15*(21), 7816. https://doi.org/10.3390/ma15217816

Joly, F.-X., & Coulis, M. (2018). Comparison of cellulose vs. plastic cigarette filter decomposition under distinct disposal environments. *Waste Management, 72*, 349–353. https://doi.org/10.1016/j.wasman.2017.11.023

Kanikireddy, V., Varaprasad, K., Jayaramudu, T., Karthikeyan, C., & Sadiku, R. (2020). Carboxymethyl cellulose-based materials for infection control and wound healing: A review. *International Journal of Biological Macromolecules, 164*, 963–975. https://doi.org/10.1016/j.ijbiomac.2020.07.160

Kim, Y., Kim, Y. K., Kim, S., Harbottle, D., & Lee, J. W. (2017). Nanostructured potassium copper hexacyanoferrate-cellulose hydrogel for selective and rapid cesium adsorption. *Chemical Engineering Journal, 313*, 1042–1050. https://doi.org/10.1016/j.cej.2016.10.136

Kim, H.-J., Kim, S.-J., Hyeon, S., Kang, H. H., & Lee, K.-Y. (2020). Application of desalination membranes to nuclide (Cs, Sr, and Co) separation. *ACS Omega, 5*(32), 20261–20269. https://doi.org/10.1021/acsomega.0c02106

Langmuir, I. (1918). The adsorption of gases on plane surfaces of glass, mica and platinum. *Journal of the American Chemical Society, 40*, 1361–1403. https://doi.org/10.1021/ja02242a004

Li, J., Wang, X., Zhao, G., Chen, C., Chai, Z., Alsaedi, A., Hayat, T., & Wang, X. (2018). Metal–organic framework-based materials: Superior adsorbents for the capture of toxic and radioactive metal ions. *Chemical Society Reviews, 47*(7), 2322–2356. https://doi.org/10.1039/C7CS00543A

Liakos, E. V., Mone, M., Lambropoulou, D. A., Bikiaris, D. N., & Kyzas, G. Z. (2021). Adsorption evaluation for the removal of nickel, mercury, and barium ions from single-component and mixtures of aqueous solutions by using an Optimized biobased chitosan derivative. *Polymers, 13*, 232. https://doi.org/10.3390/polym13020232

Mary, B. C. J., Vijaya, J. J., Bououdina, M., Khezami, L., Modwi, A., Ismail, M., & Bellucci, S. (2022). Study of barium adsorption from aqueous solutions using copper ferrite and copper ferrite/rGO magnetic adsorbents. *Adsorption Science & Technology, 2022*, 3954536. https://doi.org/10.1155/2022/3954536

McDowell, W. J., Case, G. N., Bartsch, R. A., & Czech, B. P. (1986). Solvent extraction of radium and barium cations into chloroform by a lipophilic acyclic polyether dicarboxylic acid. *Solvent Extraction and Ion Exchange, 4*, 411–419.

Miskovic-Stankovic, V., Erakovic, S., Jankovic, A., Vukasinovic-Sekulic, M., Mitric, M., Jung, Y. C., Park, S.-J., & Rhee, K. Y. (2015). Electrochemical synthesis of nanosized hydroxyapatite/graphene composite powder. *Carbon Letters, 16*(4), 233–240. https://doi.org/10.5714/CL.2015.16.4.233

Mohajerani, A., Kadir, A. A., & Larobina, L. A. (2016). Practical proposal for solving the world's cigarette butt problem: Recycling in fired clay bricks. *Waste Management, 52*, 228–244. https://doi.org/10.1016/j.wasman.2016.03.012

Möller, T., Bestaoui, N., Wierzbicki, M., Adams, T., & Clearfield, A. (2011). Separation of lanthanum, hafnium, barium and radiotracers yttrium-88 and barium-133 using crystalline zirconium phosphate and phosphonate compounds as prospective materials for a Ra-223 radioisotope generator. *Applied Radiation and Isotopes, 69*(7), 947–954. https://doi.org/10.1016/j.apradiso.2011.02.033

Monteil-Rivera, F., & Fedoroff, M. (2015). Sorption of inorganic species from solutions on apatites. In P. Somasundaran, G. Deo, R. Farinato, V. Grassian, M. Lu, M. Malmsten, K. L. Mittal, R. Nagarajan, P. Partha, G. Sukhorukov, & D. Wasan (Eds.), *Encyclopedia of surface and colloid science* (3rd ed, pp. 6787–6810). CRC Press. https://doi.org/10.1081/E-ESCS3-120010190 Retrieved December 6, 2023.

Mu, W., Du, S., Yu, Q., Li, X., Wei, H., & Yang, Y. (2018). Improving barium ion adsorption on two-dimensional titanium carbide by surface modification. *Dalton Transactions, 47*, 8375–8381. https://doi.org/10.1039/C8DT00917A

Muntean, S. G., Halip, L., Nistor, M. A., & Păcurariu, C. (2023). Removal of metal ions via adsorption using carbon magnetic nanocomposites: Optimization through response surface methodology, kinetic and thermodynamic studies. *Magnetochemistry, 9*(7), 163. https://doi.org/10.3390/magnetochemistry9070163

Murugan, K., Suresh, U., Panneerselvam, C., Rajaganesh, R., Roni, M., Hwang, J.-S., Sathishkumar, K., Rajasekar, A., Kumar, S., & Alarfaj, A. A. (2018). Managing wastes as green resources: Cigarette butt-synthesized pesticides are highly toxic to malaria vectors with little impact on predatory copepods. *Environmental Science and Pollution Research, 25*, 10456–10470. https://doi.org/10.1007/s11356-017-0074-3

Muuri, E., Mataraaho, M., Puhakka, E., Ikonen, J., Martin, A., Koskinen, L., & Siitari-Kauppi, M. (2018). The sorption and diffusion of 133Ba in crushed and intact granitic rocks from the Olkiluoto and Grimsel in-situ test sites. *Applied Geochemistry, 89*, 138–149. https://doi.org/10.1016/j.apgeochem.2017.12.004

Ng, M., Freeman, M. K., Fleming, T. D., Robinson, M., Dwyer-Lindgren, L., Thomson, B., Wollum, A., Sanman, E., Wulf, S., & Lopez, A. D. (2014). Smoking prevalence and cigarette consumption in 187 countries, 1980–2012. *JAMA, 311*, 183–192. https://doi.org/10.1001/jama.2013.284692

Noli, F., Kapnisti, M., Buema, G., & Harja, M. (2016). Retention of barium and europium radionuclides from aqueous solutions on ash-based sorbents by application of radiochemical techniques. *Applied Radiation and Isotopes, 116*, 102–109. https://doi.org/10.1016/j.apradiso.2016.07.012

Noli, F., Fedorcea, V., Misaelides, P., Cretescu, I., & Kapnisti, M. (2021). Cesium and barium removal from aqueous solutions in the presence of humic acid and competing cations by a Greek bentonite from Kimolos Island. *Applied Radiation and Isotopes, 170*, 109600. https://doi.org/10.1016/j.apradiso.2021.109600

Ogundare, S. A., Moodley, V., & van Zyl, W. E. (2017). Nanocrystalline cellulose isolated from discarded cigarette

filters. *Carbohydrate Polymers, 175*, 273–281. https://doi.org/10.1016/j.carbpol.2017.08.008

Osmanlioglu, A. E. (2018). Decontamination of radioactive wastewater by two-staged chemical precipitation. *Nuclear Engineering and Technology, 50*(6), 886–889. https://doi.org/10.1016/j.net.2018.04.009

Pérez-Madrigal, M. M., Edo, M. G., & Alemán, C. (2016). Powering the future: Application of cellulose-based materials for supercapacitors. *Green Chemistry, 18*, 5930–5956. https://doi.org/10.1039/C6GC02086K

Petersen, N., & Gatenholm, P. (2011). Bacterial cellulose-based materials and medical devices: Current state and perspectives. *Applied Microbiology and Biotechnology, 91*, 1277. https://doi.org/10.1007/s00253-011-3432-y

Poralan, G. M., Gambe, J. E., Alcantara, E. M., & Vequizo, R. M. (2015). X-Ray Diffraction and infrared spectroscopy analyses on the crystallinity of engineered biological hydroxyapatite for medical application. *IOP Conference Series: Materials Science and Engineering, 79*(1), 012028. https://doi.org/10.1088/1757-899X/79/1/012028

Reichert, J., & Binner, J. G. P. (1996). An evaluation of hydroxyapatite-based filters for removal of heavy metal ions from aqueous solutions. *Journal of Materials Science, 31*, 1231–1241. https://doi.org/10.1007/BF00353102

Roy, K., Pal, D. K., Basu, S., Nayak, D., & Lahiri, S. (2002). Synthesis of a new ion exchanger, zirconium vanadate, and its application to the separation of barium and cesium radionuclides at tracer levels. *Applied Radiation and Isotopes, 57*, 471–474. https://doi.org/10.1016/S0969-8043(02)00136-7

Sajih, M., Bryan, N. D., Livens, F. R., Vaughan, D. J., Descostes, M., Phrommavanh, V., Nos, J., & Morris, K. (2014). Adsorption of radium and barium on goethite and ferrihydrite: A kinetic and surface complexation modelling study. *Geochimica Et Cosmochimica Acta, 146*, 150–163. https://doi.org/10.1016/j.gca.2014.10.008

Salbu, B., Skipperud, L., & Lind, O. C. (2015). Sources contributing to radionuclides in the environment: with focus on radioactive particles. In C. Walther & D. Gupta (Eds.), *Radionuclides in the environment: Influence of chemical speciation and plant uptake on radionuclide migration* (pp. 1–36). Springer. https://doi.org/10.1007/978-3-319-22171-7_1

Saleeb, F. Z., & De Bruyn, P. L. (1972). Surface properties of alkaline earth apatites. *Journal of Electroanalytical Chemistry and Interfacial Electrochemistry, 37*(1), 99–118.

Sarani, N. A., & Binti Abdul Kadir, A. (2013). Thermal conductivity of fired clay bricks incorporated with cigarette butts. *Advanced Materials Research, 690*, 919–924. https://doi.org/10.4028/www.scientific.net/AMR.690-693.919

Saravanan, R., & Ravikumar, L. (2016). Cellulose bearing schiff base and carboxylic acid chelating groups: A low cost and green adsorbent for heavy metal ion removal from aqueous solution. *Water Science & Technology, 74*, 1780–1792. https://doi.org/10.2166/wst.2016.296

Skwarek, E., & Janusz, W. (2019). Adsorption of Ba^{2+} ions at the hydroxyapatite NaCl solution interface. *Adsorption, 25*(11), 279–288. https://doi.org/10.1007/s10450-018-00005-1

Sun, B., Zhang, M., Shen, J., He, Z., Fatehi, P., & Ni, Y. (2019). Applications of cellulose-based materials in sustained drug delivery systems. *Current Medicinal Chemistry, 26*, 2485–2501. https://doi.org/10.2174/0929867324666170705143308

Tellería-Narvaez, A., Talavera-Ramos, W., Dos Santos, L., Arias, J., Kinbaum, A., & Luca, V. (2020). Functionalized natural cellulose fibres for the recovery of uranium from seawater. *RSC Advances, 10*, 6654–6657. https://doi.org/10.1039/D0RA00601G

Torab-Mostaedi, M., Ghaemi, A., Ghassabzadeh, H., & Ghannadi-Maragheh, M. (2011). Removal of strontium and barium from aqueous solutions by adsorption on to expanded perlite. *The Canadian Journal of Chemical Engineering, 89*(5), 1247–1254. https://doi.org/10.1002/cjce.20486

Toraldo, E., Mariani, E., & Malvicini, S. (2015). Laboratory investigation into the effects of fibers on bituminous mixtures. *Journal of Civil Engineering and Management, 21*, 45–53. https://doi.org/10.3846/13923730.2013.802720

Wadalkar, S., Kulkarni, R., Sawant, N., Kashyap, A., Pathan, Z., & Kale, A. (2018). Design of precast concrete blocks for paving with the use of cigarette butts (cellulose acetate). *International Journal for Research in Applied Science and Engineering Technology, 6*, 2958–2965. https://doi.org/10.22214/ijraset.2018.5482

Wang, J., Liu, M., Duan, C., Sun, J., & Xu, Y. (2019). Preparation and characterization of cellulose-based adsorbent and its application in heavy metal ions removal. *Carbohydrate Polymers, 206*, 837–843. https://doi.org/10.1016/j.carbpol.2018.11.059

Xiong, Q., Bai, Q., Li, C., Lei, H., Liu, C., Shen, Y., & Uyama, H. (2018). Cost-effective, highly selective and environmentally friendly superhydrophobic absorbent from cigarette filters for oil spillage clean up. *Polymers, 10*(10), 1101. https://doi.org/10.3390/polym10101101

Xiong, Q., Bai, Q., Li, C., Li, D., Miao, X., Shen, Y., & Uyama, H. (2019). Nitrogen-doped hierarchical porous carbons from used cigarette filters for supercapacitors. *Journal of the Taiwan Institute of Chemical Engineers, 95*, 315–323. https://doi.org/10.1016/j.jtice.2018.07.019

Xu, C., Wang, J., & Chen, J. (2012). Solvent extraction of strontium and cesium: A review of recent progress. *Solvent Extraction and Ion Exchange, 30*, 623–650. https://doi.org/10.1080/07366299.2012.700579

Yue, X., Huang, J., Jiang, F., Lin, H., & Chen, Y. (2019). Synthesis and characterization of cellulose-based adsorbent for removal of anionic and cationic dyes. *Journal of Engineered Fibers and Fabrics, 2019*, 14. https://doi.org/10.1177/1558925019828194

Zaki, A. A., Hala, A. A., & Othman, E. A. (2016). Performance improvement of a radioactive forced circulation evaporator system. *Arab Journal of Nuclear Sciences and Applications, 49*(1), 76–86.

Zhao, J., Zhang, N., Qu, C., Wu, X., Zhang, J., & Zhang, X. (2010). Cigarette butts and their application in corrosion inhibition for N80 steel at 90 °C in a hydrochloric acid solution. *Industrial & Engineering Chemistry Research, 49*(8), 3986–3991. https://doi.org/10.1021/ie100168s

Zhao, X., Pei, L., Zhang, Y.-N., Huang, H., Zheng, X., Liu, B., & Tong, M. (2022). Effective and irreversible removal of radioactive barium ions in MOF-808

framework functionalized sulfonic acid groups. *Green Chemical Engineering, 3*(4), 405–412. https://doi.org/10.1016/j.gce.2022.01.007

Zhou, J., Kirk, M., Baldo, P., & Lu, F. (2021). Radiation stability of nanostructured hydroxyapatite $Ca_{10}(PO_4)_6(OH)_2$ under ion irradiations. *Journal of Nuclear Materials, 557*, 153271. https://doi.org/10.1016/j.jnucmat.2021.153271